

# Thermal properties of asymmetric nuclear matter with an improved isospin- and momentum-dependent interaction

Jun Xu,<sup>1,2,\*</sup> Lie-Wen Chen,<sup>3,4,†</sup> and Bao-An Li<sup>5,6,‡</sup><sup>1</sup>*Shanghai Institute of Applied Physics, Chinese Academy of Sciences, Shanghai 201800, China*<sup>2</sup>*Kavli Institute for Theoretical Physics, Chinese Academy of Sciences, Beijing 100190, China*<sup>3</sup>*Department of Physics and Astronomy and Shanghai Key Laboratory for Particle Physics and Cosmology, Shanghai Jiao Tong University, Shanghai 200240, China*<sup>4</sup>*Center of Theoretical Nuclear Physics, National Laboratory of Heavy Ion Accelerator, Lanzhou 730000, China*<sup>5</sup>*Department of Physics and Astronomy, Texas A&M University-Commerce, Commerce, Texas 75429-3011, USA*<sup>6</sup>*Department of Applied Physics, Xi'an Jiao Tong University, Xi'an 710049, China*

(Received 6 October 2014; published 21 January 2015)

Thermal properties of asymmetric nuclear matter, including the temperature dependence of the symmetry energy, single-particle properties, and differential isospin fractionation, are investigated with different neutron-proton effective mass splittings by using an improved isospin- and momentum-dependent interaction. In this improved interaction, the momentum dependence of the isoscalar single-particle potential at saturation density is well fit to that extracted from optical-model analyses of proton-nucleus scattering data up to the nucleon kinetic energy of 1 GeV, and the isovector properties, i.e., the slope of the nuclear symmetry energy, the momentum dependence of the symmetry potential, and the symmetry energy at saturation density, can be flexibly adjusted via three parameters:  $x$ ,  $y$ , and  $z$ , respectively. Our results indicate that the nucleon phase-space distribution in equilibrium, the temperature dependence of the symmetry energy, and the differential isospin fractionation can be significantly affected by the isospin splitting of the nucleon effective mass.

DOI: [10.1103/PhysRevC.91.014611](https://doi.org/10.1103/PhysRevC.91.014611)

PACS number(s): 21.65.-f, 21.30.Fe, 24.10.Pa, 64.10.+h

## I. INTRODUCTION

Understanding the in-medium nucleon-nucleon (NN) interaction is one of the main tasks of nuclear physics. The single-particle potential of a nucleon in the nuclear medium is closely related to the NN interaction as well as to the properties of nuclear matter. Based on the Brueckner theory, the potential of a nucleon depends not only on the properties of the medium but also on the momentum of the nucleon, and the momentum dependence comes from the exchange contribution of the finite-range NN interaction within the Hartree-Fock framework. More than twenty years ago, for studying heavy-ion collisions, the momentum-dependent mean-field potential was gradually improved from the Gale-Bertsch-Das Gupta (GBD) interaction [1] to a momentum-dependent Yukawa interaction (MDYI) [2,3]. Later, the isospin dependence was further introduced to the momentum-dependent potential and the newly developed interaction was named MDI [4]. It was found that the momentum dependence of the nucleon potential affects not only the dynamics of heavy-ion collisions (see Ref. [5] for a review), but also the thermodynamic properties of nuclear matter as well [6,7]. This interaction has further been used to study the core-crust transition density of neutron stars [8–10] and to study the properties of hybrid stars after it was extended to include hyperon interactions [11]. Moreover, the MDI together with an isospin-dependent Boltzmann-Uehling-Uhlenbeck transport model was used to study the symmetry

energy at both subsaturation [12] and suprasaturation densities [13]. For the latest review of the MDI interaction, we refer the reader to Ref. [14].

The above MDI interaction was further improved in 2010 [15], and the new interaction, dubbed ImMDI, mainly includes the following three improvements: First, the single-particle potential in symmetric nuclear matter at  $\rho_0$  was refit to reproduce the empirical optical potential [16,17] up to nucleon kinetic energy of 1 GeV, while that in the previous MDI interaction becomes more attractive than that extracted from the proton-nucleus scattering data at nucleon momenta larger than about 550 MeV/c (i.e., the nucleon kinetic energy of about 160 MeV), as can be seen from Fig. 2 of Ref. [11]. Second, a parameter  $y$  was introduced to mimic the momentum dependence of the symmetry potential or, equivalently, the isospin splitting of the nucleon effective mass. Third, considering that the isospin tracers are sensitive to both the slope parameter  $L$  of the symmetry energy (mimicked by the parameter  $x$  in the MDI interaction) and the symmetry energy  $E_{\text{sym}}(\rho_0)$  at the saturation density and the constraints of the nuclear symmetry energy are usually mapped in the  $L \sim E_{\text{sym}}(\rho_0)$  plane (see, e.g., Fig. 1 of Ref. [18] and Fig. 2 of Ref. [19]), a parameter  $z$  is introduced to vary the value of  $E_{\text{sym}}(\rho_0)$ . The ImMDI can thus describe more reliably the dynamics of heavy-ion collisions at beam energies up to 1 GeV and provide possibilities to study simultaneously more detailed isovector properties of nuclear matter, such as the slope parameter of the symmetry energy, the momentum dependence of the symmetry potential, and the symmetry energy at saturation density.

The neutron-proton effective-mass splitting has been studied for a long time [20–24] and has recently become again a

\*xujun@sinap.ac.cn

†lwchen@sjtu.edu.cn

‡bao-an.li@tamuc.edu

hot topic [25–34]. It is noteworthy that, in relativistic models, one needs to calculate the Lorentz mass so that it can be compared with that from the nonrelativistic interactions. For Lorentz effective mass, the microscopic Brueckner–Hartree–Fock or Dirac–Brueckner–Hartree–Fock approach and most Skyrme–Hartree–Fock calculations lead to a larger neutron effective mass than proton effective mass in neutron-rich nuclear matter, while most relativistic mean-field models and a few Skyrme–Hartree–Fock calculations give opposite predictions. The larger neutron effective mass than proton effective mass requires that the nuclear symmetry potential decreases with increasing nucleon momentum or energy, which is more consistent with the Lane potential in trend [22]. In addition, the neutron clearly has a larger effective mass than the proton in neutron-rich matter based on optical-model analyses for nucleon-nucleus elastic scattering [31,32,35]. On the other hand, the recent experimental data of the double neutron/proton ratio from the National Superconducting Cyclotron Laboratory seems to favor a smaller neutron effective mass than proton effective mass based on the calculation using an improved quantum molecular dynamics model [36], although short-range correlations might be another alternative explanation [37]. Since the possibility of a smaller neutron effective mass than proton effective mass in neutron-rich matter has not been absolutely ruled out yet and is currently hotly debated, it is of great interest to study in more detail the possible effects from different neutron-proton effective-mass splittings. It was found that the dynamic properties in heavy-ion collisions can be affected by the isospin splitting of nucleon effective mass and the latter has considerable effect on the single and double neutron/proton ratio,  $t/{}^3\text{He}$  ratio, and isospin-dependent collective flows and particle productions [23–26,28,29,33,34]. In the present paper, we study the effects on thermodynamical properties of nuclear matter from different isospin splittings of nucleon effective mass based on the ImMDI.

## II. IMPROVED ISOSPIN- AND MOMENTUM-DEPENDENT INTERACTION

The functional form of potential energy density of nuclear matter for the ImMDI is the same as the MDI [4,12], i.e.,

$$\begin{aligned}
 V(\rho, \delta) = & \frac{A_u \rho_n \rho_p}{\rho_0} + \frac{A_l}{2\rho_0} (\rho_n^2 + \rho_p^2) + \frac{B}{\sigma + 1} \frac{\rho^{\sigma+1}}{\rho_0^\sigma} \\
 & \times (1 - x\delta^2) + \frac{1}{\rho_0} \sum_{\tau, \tau'} C_{\tau, \tau'} \\
 & \times \iint d^3 p d^3 p' \frac{f_\tau(\vec{r}, \vec{p}) f_{\tau'}(\vec{r}, \vec{p}')}{1 + (\vec{p} - \vec{p}')^2 / \Lambda^2}. \quad (1)
 \end{aligned}$$

In the mean-field approximation, Eq. (1) leads to the following single-particle potential [4,12]:

$$\begin{aligned}
 U_\tau(\rho, \delta, \vec{p}) = & A_u \frac{\rho_{-\tau}}{\rho_0} + A_l \frac{\rho_\tau}{\rho_0} \\
 & + B \left( \frac{\rho}{\rho_0} \right)^\sigma (1 - x\delta^2) - 4\tau x \frac{B}{\sigma + 1} \frac{\rho^{\sigma-1}}{\rho_0^\sigma} \delta \rho_{-\tau}
 \end{aligned}$$

$$\begin{aligned}
 & + \frac{2C_l}{\rho_0} \int d^3 p' \frac{f_\tau(\vec{r}, \vec{p}')}{1 + (\vec{p} - \vec{p}')^2 / \Lambda^2} \\
 & + \frac{2C_u}{\rho_0} \int d^3 p' \frac{f_{-\tau}(\vec{r}, \vec{p}')}{1 + (\vec{p} - \vec{p}')^2 / \Lambda^2}. \quad (2)
 \end{aligned}$$

In the above,  $\rho_n$  and  $\rho_p$  are number densities of neutrons and protons, respectively, and the isospin asymmetry  $\delta$  is defined as  $\delta = (\rho_n - \rho_p) / \rho$ , with  $\rho = \rho_n + \rho_p$  being the total number density.  $f_\tau(\vec{r}, \vec{p})$  is the phase-space distribution function, with  $\tau = 1 (-1)$  for neutrons (protons) being the isospin index.

The seven parameters ( $A_l, A_u, B, C_l = C_{\tau, \tau}, C_u = C_{\tau, -\tau}, \Lambda, \sigma$ ) can be fit by seven empirical constraints. Typically, five isoscalar constraints of the saturation density  $\rho_0$ , the binding energy  $E_0$ , the incompressibility  $K_0$ , the isoscalar effective mass  $m_s^*$ , and the single-particle potential  $U_{0, \infty}$  at infinitely large nucleon momentum at saturation density in symmetric nuclear matter can be determined by  $A_l + A_u, B, C_l + C_u, \Lambda$ , and  $\sigma$ . In addition, two isovector constraints of the symmetry energy  $E_{\text{sym}}(\rho_0)$  and the symmetry potential  $U_{\text{sym}, \infty}$  at infinitely large nucleon momentum (or equivalently the neutron-proton effective-mass splitting) at saturation density can be determined by  $A_l - A_u$  and  $C_l - C_u$ . In addition to the  $x$  parameter in the previous MDI, which can be used to adjust the slope parameter  $L$  of the symmetry energy at saturation density, we introduce two additional parameters  $y$  and  $z$  to adjust respectively  $U_{\text{sym}, \infty}$  and  $E_{\text{sym}}(\rho_0)$ , and  $A_l, A_u, C_l$ , and  $C_u$  can then be expressed as

$$A_l(x, y) = A_{l0} + y + x \frac{2B}{\sigma + 1}, \quad (3)$$

$$A_u(x, y) = A_{u0} - y - x \frac{2B}{\sigma + 1}, \quad (4)$$

$$C_l(y, z) = C_{l0} - 2(y - 2z) \frac{p_{f0}^2}{\Lambda^2 \ln[(4p_{f0}^2 + \Lambda^2)/\Lambda^2]}, \quad (5)$$

$$C_u(y, z) = C_{u0} + 2(y - 2z) \frac{p_{f0}^2}{\Lambda^2 \ln[(4p_{f0}^2 + \Lambda^2)/\Lambda^2]}, \quad (6)$$

where  $p_{f0}$  is the nucleon Fermi momentum in symmetric nuclear matter at saturation density. For  $x = 0, y = 0$ , and  $z = 0$ , we choose the following empirical values:  $\rho_0 = 0.16 \text{ fm}^{-3}$ ,  $E_0(\rho_0) = -16 \text{ MeV}$ ,  $K_0 = 230 \text{ MeV}$ ,  $m_s^* = 0.7m$ ,  $E_{\text{sym}}(\rho_0) = 32.5 \text{ MeV}$ , and  $U_{0, \infty} = 75 \text{ MeV}$ , which lead to  $A_{l0} = A_{u0} = -66.963 \text{ MeV}$ ,  $B = 141.963 \text{ MeV}$ ,  $C_{l0} = -60.4860 \text{ MeV}$ ,  $C_{u0} = -99.7017 \text{ MeV}$ ,  $\Lambda = 2.42401 p_{f0}$ , and  $\sigma = 1.26521$ . Again, the values of  $x, y$ , and  $z$  only affect the isovector properties of nuclear matter but do not lead to the variation of the empirical isoscalar constraints.

The potential-energy density functional of Eq. (1) can be obtained from the following effective NN interaction within the Hartree–Fock approach [4,38]:

$$\begin{aligned}
 v(\vec{r}_1, \vec{r}_2) = & \frac{1}{6} t_3 (1 + x_3 P_\sigma) \rho^\gamma \left( \frac{\vec{r}_1 + \vec{r}_2}{2} \right) \delta(\vec{r}_1 - \vec{r}_2) \\
 & + (W + G P_\sigma - H P_\tau - M P_\sigma P_\tau) \frac{e^{-\mu|\vec{r}_1 - \vec{r}_2|}}{|\vec{r}_1 - \vec{r}_2|}; \quad (7)
 \end{aligned}$$

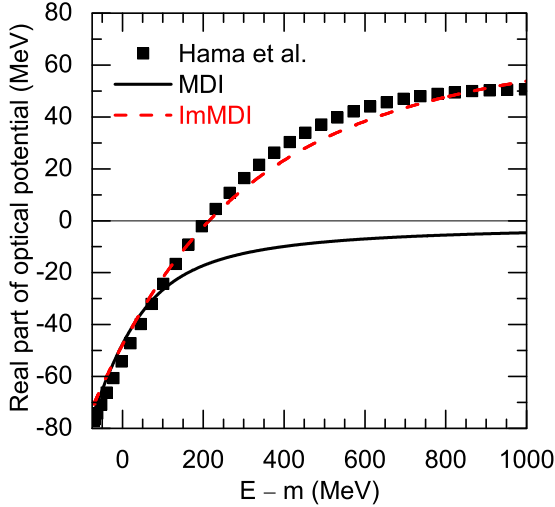


FIG. 1. (Color online) The ImMDI prediction for the single-particle potential in symmetric nuclear matter at  $\rho_0$  as a function of nucleon total energy with its rest mass subtracted. The results of the MDI and the optical potential by Hama *et al.* [16,17] are also shown for comparison.

namely, a density-dependent zero-range interaction and a finite-range Yukawa-type two-body interaction, with  $\vec{r}_1$  and  $\vec{r}_2$  being the spatial coordinates of the two nucleons and  $P_\sigma$  and  $P_\tau$  being the spin and isospin exchange operators, respectively. The values of the parameters  $t_3$ ,  $\gamma$ ,  $W$ ,  $G$ ,  $H$ ,  $M$ , and  $\mu$  can be uniquely determined from  $A_l$ ,  $A_u$ ,  $B$ ,  $C_l$ ,  $C_u$ ,  $\Lambda$ , and  $\sigma$  [38]. The  $x$  parameter is related to the value of  $x_3$ , i.e., the relative contribution of the isospin-singlet and the isospin-triplet channel of the density-dependent interaction, while the values of  $y$  and  $z$  are related to those of  $W$ ,  $G$ ,  $H$ , and  $M$  and are thus determined by the different spin-isospin channels of the finite-range interaction.

In the ImMDI,  $U_{0,\infty} = (A_l + A_u)/2 + B = 75$  MeV is selected to fit the empirical optical potential of Hama *et al.*, and this can be seen from Fig. 1 where the single-particle potential (i.e., the real part of the optical potential) in symmetric nuclear matter at  $\rho_0$  is plotted as a function of nucleon total energy with its rest mass subtracted, i.e.,  $E - m$ . The results of the MDI and the optical potential by Hama *et al.* [16,17] are also shown for comparison. One can see that the MDI, whose momentum dependence of the mean-field potential is fit to reproduce that of the Gogny interaction, significantly underpredicts the empirical optical potential by Hama *et al.* when  $E - m$  is larger than about 160 MeV. We note that the wrong asymptotic value of the isoscalar potential at high momentum is actually a longstanding problem of the Gogny effective interaction. On the other hand, the energy and momentum dependence of the single-particle potential in symmetric nuclear matter at  $\rho_0$  predicted by the ImMDI is in good agreement with the empirical optical potential by Hama *et al.* in the whole energy region up to about  $E - m = 1000$  MeV. Therefore, the ImMDI provides a reasonable choice for the transport-model simulations for heavy-ion collisions at low and intermediate energies (up to at least about 1 GeV/nucleon).

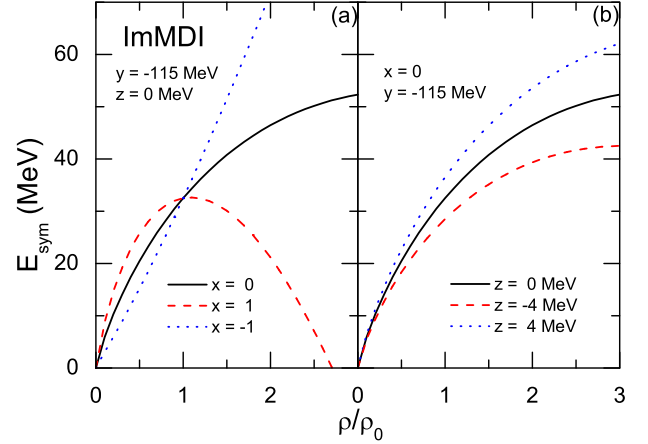


FIG. 2. (Color online) The symmetry energy from the ImMDI by (a) adjusting the value of parameter  $x$  at  $y = -115$  MeV and  $z = 0$  MeV or (b) parameter  $z$  at  $x = 0$  and  $y = -115$  MeV.

In the ImMDI, one can vary flexibly three parameters, i.e.,  $x$ ,  $y$ , and  $z$  to change the isovector properties of nuclear matter. Similar to the previous MDI interaction, the density dependence of the symmetry energy (e.g., the slope parameter  $L$ ) changes with the parameters  $x$  while  $E_{\text{sym}}(\rho_0)$  remains unchanged, as can be seen from the left panel of Fig. 2. On the other hand, the value of the symmetry energy at saturation density changes from  $E_{\text{sym}}(\rho_0)$  to  $E_{\text{sym}}(\rho_0) + z$  when  $z$  is adjusted, as can be seen from the right panel of Fig. 2. In this way one can easily study the sensitivity of the isospin tracers to the values of  $L$  and  $E_{\text{sym}}(\rho_0)$  simultaneously. In addition, one can vary the  $y$  parameter, which is equivalent to  $U_{\text{sym},\infty}$ , to modify the momentum dependence of the symmetry potential  $U_{\text{sym}}(\rho, p)$  at  $\rho_0$  (and also other densities), while in the MDI interaction, the momentum dependence of  $U_{\text{sym}}(\rho, p)$  is fixed although the magnitude of  $U_{\text{sym}}(\rho, p)$  at nonsaturation densities can be varied by using different  $x$  values. It is clearly seen from the left panel of Fig. 3 that one can flexibly vary the  $y$  parameter to mimic different momentum or energy dependencies of  $U_{\text{sym}}(\rho, p)$  (and thus the isospin splitting of the nucleon effective mass), providing a convenient way

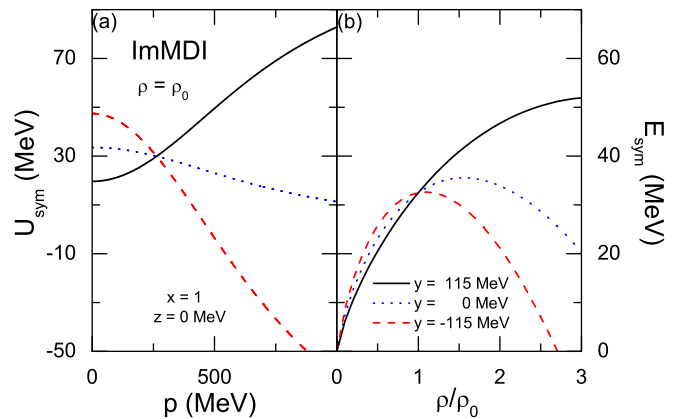


FIG. 3. (Color online) (a) The symmetry potential at saturation density and (b) symmetry energy from the ImMDI by adjusting the value of parameter  $y$  at  $x = 1$  and  $z = 0$  MeV.

to explore the consequent effects in heavy-ion collisions. In addition, one can see  $U_{\text{sym}}(\rho_0, p)$  at  $p = p_{f0}$  (corresponding to a nucleon kinetic energy of 36.8 MeV) is independent of the  $y$  parameter by construction. On the other hand, it is seen from the right panel of Fig. 3 that the density dependence of the symmetry energy changes with  $y$  as well, with the values of  $E_{\text{sym}}(\rho_0)$  fixed. This can be understood because the slope parameter  $L$  depends not only on the magnitude of symmetry potential, which is related to the  $x$  parameter, but also on the momentum dependence of the symmetry potential [35,39].

### III. EFFECTS OF NEUTRON-PROTON EFFECTIVE-MASS SPLITTING

The ImMDI described in the previous section provides possibilities of flexibly studying more detailed isovector properties of nuclear matter. In the following, we study the effects of neutron-proton effective-mass splitting on thermodynamic properties of neutron-rich nuclear matter. One can see from Figs. 2 and 3 that  $[(x = 0), (y = -115 \text{ MeV})]$  and  $[(x = 1), (y = 115 \text{ MeV})]$  give almost the same density dependence of the symmetry energy at  $z = 0$ , whereas the two parameter sets lead to two extreme momentum dependencies of the symmetry potential, with  $U_{\text{sym}}$  from  $[(x = 0), (y = -115 \text{ MeV})]$  decreasing with increasing nucleon momentum and thus  $m_n^* > m_p^*$  and that from  $[(x = 1), (y = 115 \text{ MeV})]$  increasing with increasing nucleon momentum and thus  $m_n^* < m_p^*$ . We will carry out our study based on the two parameter sets in the following.

#### A. Temperature dependence of symmetry energy

Because from Eq. (2) the single-particle potential depends on the phase-space distribution function, and from the single-particle approximation this Fermi–Dirac phase-space distribution function in equilibrium depends on the single-particle potential, an iteration method is needed to calculate the mean-field potential and the equation of state at finite temperature [40]. From such a self-consistent calculation, the equilibrated phase-space distribution functions of neutrons and protons for  $[(x = 0), (y = -115 \text{ MeV})]$  and  $[(x = 1), (y = 115 \text{ MeV})]$  in neutron-rich nuclear matter of isospin asymmetry  $\delta = 0.5$  at saturation density and temperature  $T = 30 \text{ MeV}$  are displayed in Fig. 4. It is seen that  $[(x = 0), (y = -115 \text{ MeV})]$ , giving a larger neutron effective mass than proton effective mass, has a more diffusive distribution for neutrons and a less diffusive distribution for protons compared with  $[(x = 1), (y = 115 \text{ MeV})]$ . This is understandable because the self-consistent calculation balances the energy of the system at fixed isospin asymmetry, so for a larger neutron (proton) effective mass than proton (neutron) effective mass with  $[(x = 0), (y = -115 \text{ MeV})]$  ( $[(x = 1), (y = 115 \text{ MeV})]$ ) more neutrons (protons) are allowed to occupy the high-momentum states.

As a key quantity of isospin physics, the density dependence of the symmetry energy for  $[(x = 0), (y = -115 \text{ MeV})]$  and  $[(x = 1), (y = 115 \text{ MeV})]$  at different temperatures is shown in Fig. 5. At finite temperatures the symmetry energy is calculated numerically by taking the difference in the binding energy between  $\delta = 0$  and  $\delta = 0.2$ . One can see for

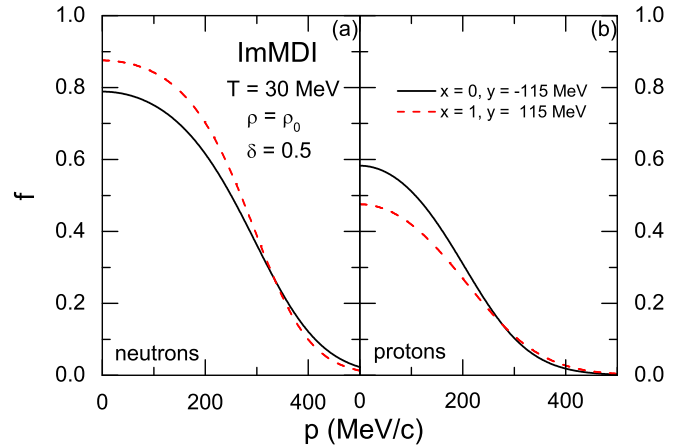


FIG. 4. (Color online) The equilibrated phase-space distribution functions (normalized by the spin degeneracy) of (a) neutrons and (b) protons from the ImMDI for  $[(x = 0), (y = -115 \text{ MeV})]$  and  $[(x = 1), (y = 115 \text{ MeV})]$  in neutron-rich nuclear matter of isospin asymmetry  $\delta = 0.5$  at saturation density and temperature  $T = 30 \text{ MeV}$ .

$[(x = 0), (y = -115 \text{ MeV})]$  that the symmetry energy decreases with increasing temperature at lower densities but slightly increases with increasing temperature at higher densities, while for  $[(x = 1), (y = 115 \text{ MeV})]$  the symmetry energy decreases with increasing temperature at all the densities. Similar behavior was observed in Ref. [26] based on the Skyrme–Hartree–Fock functional. To understand the different temperature dependence of the symmetry energy with different isospin splitting of nucleon effective mass, we further show in Figs. 6 and 7 the kinetic and potential contribution to the symmetry energy, respectively. It is interesting to see that the kinetic contribution to the symmetry energy increases with increasing temperature for  $[(x = 0), (y = -115 \text{ MeV})]$  but decreases with increasing temperature for  $[(x = 1), (y = 115 \text{ MeV})]$ . This is because there are more neutrons and less protons in the high-energy states with increasing temperature

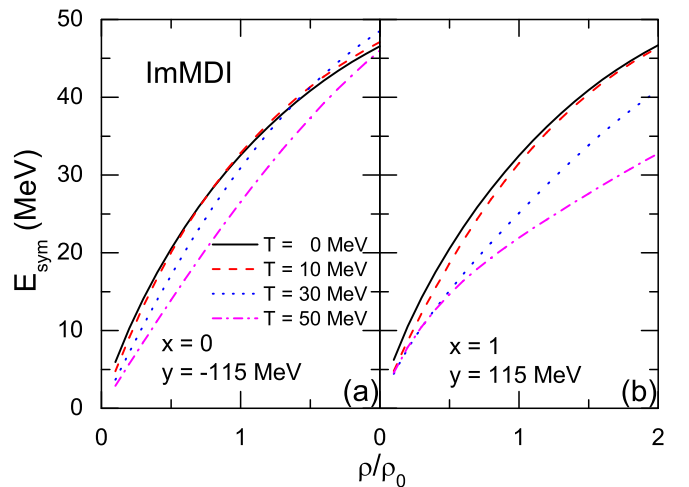


FIG. 5. (Color online) The nuclear symmetry energy from the ImMDI for (a)  $[(x = 0), (y = -115 \text{ MeV})]$  and (b)  $[(x = 1), (y = 115 \text{ MeV})]$  at temperatures of 0, 10, 30, and 50 MeV.

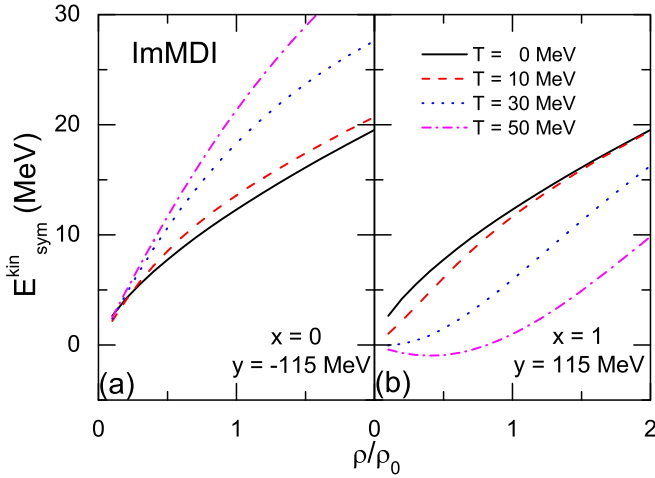


FIG. 6. (Color online) Same as Fig. 5 but only for the kinetic contribution of the symmetry energy.

for  $[(x = 0), (y = -115 \text{ MeV})]$  but it is opposite for  $[(x = 1), (y = 115 \text{ MeV})]$ , as can be seen from Fig. 4. For the potential contribution to the symmetry energy, it somehow decreases with increasing temperature for  $[(x = 0), (y = -115 \text{ MeV})]$  but has a weak temperature dependence for  $[(x = 1), (y = 115 \text{ MeV})]$ . The combination of Figs. 6 and 7 leads to the temperature dependence of the total symmetry energy in Fig. 5.

### B. Isovector single-particle properties

We now move to the isovector single-particle properties of nuclear matter including the symmetry potential and the neutron-proton effective-mass splitting. The momentum dependence of the symmetry potential for  $[(x = 0), (y = -115 \text{ MeV})]$  and  $[(x = 1), (y = 115 \text{ MeV})]$  at different densities and temperatures is shown in Fig. 8, and the results are calculated by taking the potential difference of neutrons and protons at  $\delta = 0.2$ . One can see that the symmetry potential decreases with increasing momentum for  $[(x = 0),$

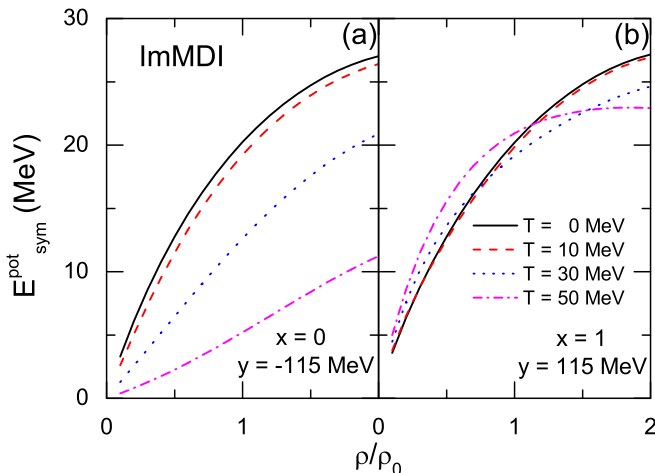


FIG. 7. (Color online) Same as Fig. 5 but only for the potential contribution of the symmetry energy.

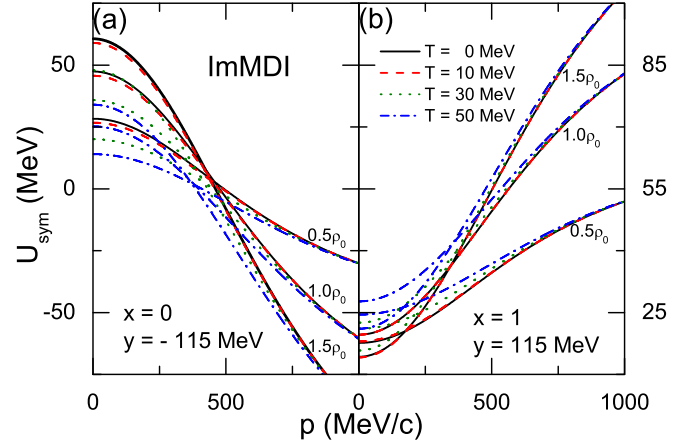


FIG. 8. (Color online) The momentum dependence of the symmetry potential from the ImMDI for (a)  $[(x = 0), (y = -115 \text{ MeV})]$  and (b)  $[(x = 1), (y = 115 \text{ MeV})]$  at different densities and temperatures.

$(y = -115 \text{ MeV})]$  but increases with increasing momentum for  $[(x = 1), (y = 115 \text{ MeV})]$ , and the slope is larger at higher densities. The symmetry potential becomes negative at high nucleon momenta for  $[(x = 0), (y = -115 \text{ MeV})]$  while it is always positive for  $[(x = 1), (y = 115 \text{ MeV})]$ . With increasing temperature, only the low-momentum part of the symmetry potential is affected while the high-momentum part remains almost unchanged. It is interesting to see that symmetry potential decreases with increasing temperature for  $[(x = 0), (y = -115 \text{ MeV})]$  while it increases with increasing temperature for  $[(x = 1), (y = 115 \text{ MeV})]$ .

A positive symmetry potential gives repulsive force to neutrons and attractive force to protons, while the velocity of the nucleon depends not only on the force but also on the in-medium effective mass. The nucleon effective mass, which is defined as

$$\frac{m_\tau^*}{m} = \left( 1 + \frac{m}{p} \frac{dU_\tau}{dp} \right)^{-1}, \quad (8)$$

is a function of nucleon momentum but is mostly represented by the value at Fermi momentum. The relative neutron-proton effective-mass splitting for  $[(x = 0), (y = -115 \text{ MeV})]$  and  $[(x = 1), (y = 115 \text{ MeV})]$  in neutron-rich nuclear matter of isospin asymmetry  $\delta = 0.5$  at different densities and temperatures is shown in Fig. 9. Indeed, the neutron effective mass is larger than that for protons for  $[(x = 0), (y = -115 \text{ MeV})]$  and smaller than that for protons for  $[(x = 1), (y = 115 \text{ MeV})]$  at all the densities and temperatures. Generally, the relative effective-mass splitting is smaller at higher nucleon momenta and stronger at higher densities, and the splitting becomes weaker at higher temperatures for  $[(x = 0), (y = -115 \text{ MeV})]$  but the temperature dependence is somehow complicated for  $[(x = 1), (y = 115 \text{ MeV})]$ , especially at higher densities.

### C. Differential isospin fractionation

The two phases of nuclear matter can coexist if the Gibbs condition is satisfied, i.e., they have the same temperature,

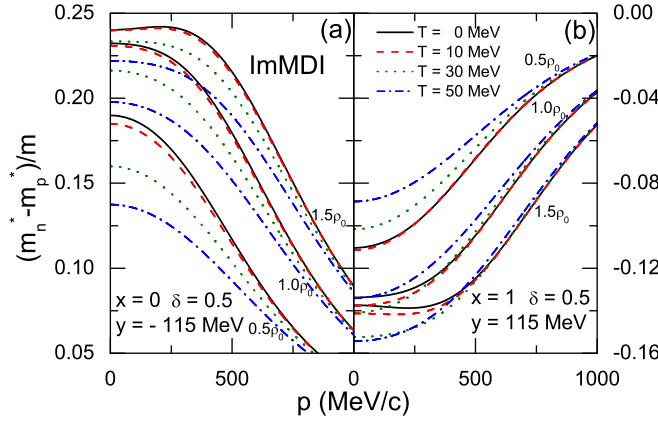


FIG. 9. (Color online) The relative neutron-proton effective mass splitting from the ImMDI for (a)  $[(x = 0), (y = -115 \text{ MeV})]$  and (b)  $[(x = 1), (y = 115 \text{ MeV})]$  in neutron-rich nuclear matter of isospin asymmetry  $\delta = 0.5$  at different densities and temperatures.

pressure, and chemical potential. The dense phase with smaller isospin asymmetry is called the liquid phase, while the dilute phase with larger isospin asymmetry is called the gas phase. As the symmetry energy generally increases with increasing density, at least at subsaturation densities, the high-density phase should have a smaller isospin asymmetry while the low-density phase can have a larger isospin asymmetry, so in this way the total energy can be well distributed in the two phases and reach a minimum value. This is the so-called isospin fractionation.

Numerically, the binodal surface of the nuclear liquid-gas phase transition can be constructed by drawing rectangles in the chemical potential isobars of neutrons and protons as functions of isospin asymmetry at a given temperature [41,42]. The two phases obtained thus satisfy the Gibbs condition, with the one of larger isospin asymmetry corresponding to the gas phase and that of the smaller isospin asymmetry corresponding to the liquid phase. Collecting all such pairs at each pressure forms the binodal surface of the nuclear liquid-gas phase transition, as shown in the left panel of Fig. 10 at the temperature  $T = 10 \text{ MeV}$ . The binodal surface is useful in calculating the volume fraction of each phase and studying the properties of nuclear liquid-gas phase transition at fixed isospin asymmetry, as shown in Ref. [7], and the liquid phase (L), the gas phase (G), and the mixed phase (M) are denoted in the figure. One can see that the binodal surface is similar for  $[(x = 0), (y = -115 \text{ MeV})]$  and  $[(x = 1), (y = 115 \text{ MeV})]$ . This is not surprising because both the chemical potential and the pressure are determined from the equation of state, which is almost the same for the two parameter sets. The slight difference is expected to be due to the different temperature dependence of the symmetry energy.

Similar to Ref. [43], we study the differential isospin fractionation at pressure  $P = 0.1 \text{ MeV}/\text{fm}^3$ . As can be seen from the left panel of Fig. 10, the nuclear matter in the mixed-phase region at  $P = 0.1 \text{ MeV}/\text{fm}^3$  comprises the liquid phase and the gas phase at two edges of the binodal surface with the same pressure. For  $[(x = 0), (y = -115 \text{ MeV})]$ , the densities and isospin asymmetries of the liquid and gas phases are

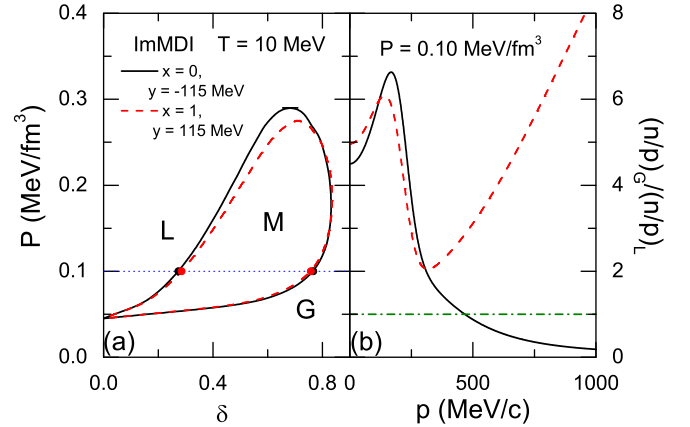


FIG. 10. (Color online) Left panel shows the section of binodal surface from the ImMDI for  $[(x = 0), (y = -115 \text{ MeV})]$  and  $[(x = 1), (y = 115 \text{ MeV})]$  at a temperature  $T = 10 \text{ MeV}$ . L, G, and M represent the liquid phase, the gas phase, and the mixed phase, respectively. Right panel shows the double neutron/proton ratio in gas and liquid phases  $(n/p)_G/(n/p)_L$  at the pressure of  $0.10 \text{ MeV}/\text{fm}^3$  as a function of nucleon momentum.

$\rho_L = 0.757\rho_0$ ,  $\delta_L = 0.273$ ,  $\rho_G = 0.087\rho_0$ , and  $\delta_G = 0.766$ , respectively. For  $[(x = 1), (y = 115 \text{ MeV})]$ , the densities and isospin asymmetries of the liquid and gas phases are  $\rho_L = 0.752\rho_0$ ,  $\delta_L = 0.285$ ,  $\rho_G = 0.083\rho_0$ , and  $\delta_G = 0.758$ , respectively. Thus, the ratios of neutron to proton in the gas phase to that in the liquid phase, i.e.,  $(n/p)_G/(n/p)_L$ , are 4.31 for  $[(x = 0), (y = -115 \text{ MeV})]$  and 4.04 for  $[(x = 1), (y = 115 \text{ MeV})]$ . Although the total ratios are similar for the two parameter sets, the differential behaviors, i.e., the momentum dependence, are quite different, as can be seen from the right panel of Fig. 10. Similar to the findings in Ref. [43], the ratio  $(n/p)_G/(n/p)_L$  becomes less than unity when the nucleon momentum is larger than about 500 MeV/c. This can be understood by checking with the symmetry potential in Fig. 8 that  $U_{\text{sym}}$  becomes negative when the nucleon momentum is larger than about 500 MeV/c. For  $[(x = 1), (y = 115 \text{ MeV})]$ , since the symmetry potential is always positive and is larger at higher nucleon momenta, the ratio  $(n/p)_G/(n/p)_L$  is always greater than unity and increases with increasing momentum at higher nucleon energies. In intermediate-energy heavy-ion collisions, the gas phase is formed by free nucleons while the liquid phase is formed by those in heavy clusters. Consistent with the finding here, it was shown in Refs. [23,24,29,33] that the neutron-to-proton ratio of energetic nucleons is sensitive to the neutron-proton effective-mass splitting.

#### IV. SUMMARY

Based on an improved isospin- and momentum-dependent interaction, with the isoscalar single-nucleon potential refit to that extracted by optical-model analyses of proton-nucleus scattering data up to the nucleon kinetic energy of about 1 GeV/c, and three parameters included for studying the detailed isovector properties of nuclear matter, i.e., the slope parameter of the symmetry energy, the momentum dependence of the symmetry potential, and the symmetry energy at

saturation density, we studied the thermodynamical properties of neutron-rich nuclear matter with the same equation of state but different neutron-proton effective-mass splittings. We find that the phase-space distribution in equilibrium, the temperature dependence of the symmetry energy, and the differential isospin fractionation can be affected by the isospin splitting of nucleon effective mass.

### ACKNOWLEDGMENTS

This work was supported in part by the Major State Basic Research Development Program (973 program) in China under Contracts No. 2015CB856904, No. 2014CB845401, and No. 2013CB834405, the National Natural Science Foundation of China under Grants No. 11475243, No. 11421505,

No. 11275125, No. 11135011, and No. 11320101004, the “100-talent plan” of the Shanghai Institute of Applied Physics under Grant No. Y290061011 from the Chinese Academy of Sciences, the “Shanghai Pujiang Program” under Grant No. 13PJ1410600, the Shu Guang project supported by Shanghai Municipal Education Commission and Shanghai Education Development Foundation, the Program for Professor of Special Appointment (Eastern Scholar) at Shanghai Institutions of Higher Learning, the Science and Technology Commission of Shanghai Municipality (11DZ2260700), the US National Science Foundation Grants No. PHY-1068022, the National Aeronautics and Space Administration under Grant No. NNX11AC41G issued through the Science Mission Directorate, and the CUSTIPEN (China-U.S. Theory Institute for Physics with Exotic Nuclei) under DOE Grant No. DE-FG02-13ER42025.

- 
- [1] C. Gale, G. Bertsch, and S. Das Gupta, *Phys. Rev. C* **35**, 1666 (1987).
- [2] G. M. Welke, M. Prakash, T. T.S. Kuo, S. Das Gupta, and C. Gale, *Phys. Rev. C* **38**, 2101 (1988).
- [3] C. Gale, G. M. Welke, M. Prakash, S. J. Lee, and S. Das Gupta, *Phys. Rev. C* **41**, 1545 (1990).
- [4] C. B. Das, S. Das Gupta, C. Gale, and B. A. Li, *Phys. Rev. C* **67**, 034611 (2003).
- [5] B. A. Li, L. W. Chen, and C. M. Ko, *Phys. Rep.* **464**, 113 (2008).
- [6] V. K. Mishra, G. Fai, L. P. Csernai, and E. Osnes, *Phys. Rev. C* **47**, 1519 (1993).
- [7] J. Xu, L. W. Chen, B. A. Li, and H. R. Ma, *Phys. Rev. C* **77**, 014302 (2008).
- [8] J. Xu, L. W. Chen, B. A. Li, and H. R. Ma, *Phys. Rev. C* **79**, 035802 (2009).
- [9] J. Xu, L. W. Chen, B. A. Li, and H. R. Ma, *Astrophys. J.* **697**, 1549 (2009).
- [10] J. Xu, L. W. Chen, C. M. Ko, and B. A. Li, *Phys. Rev. C* **81**, 055805 (2010).
- [11] J. Xu, L. W. Chen, C. M. Ko, and B. A. Li, *Phys. Rev. C* **81**, 055803 (2010).
- [12] L. W. Chen, C. M. Ko, and B. A. Li, *Phys. Rev. Lett.* **94**, 032701 (2005).
- [13] Z. G. Xiao, B. A. Li, L. W. Chen, G. C. Yong, and M. Zhang, *Phys. Rev. Lett.* **102**, 062502 (2009).
- [14] L. W. Chen, C. M. Ko, B. A. Li, C. Xu, and J. Xu, *Eur. Phys. J. A* **50**, 29 (2014).
- [15] L. W. Chen and B. A. Li, *A Note of an Improved MDI Interaction for Transport Model Simulations of Heavy Ion Collisions* (Texas A&M University-Commerce, 2010) (unpublished).
- [16] S. Hama, B. C. Clark, E. D. Cooper, H. S. Sherif, and R. L. Mercer, *Phys. Rev. C* **41**, 2737 (1990).
- [17] E. D. Cooper, S. Hama, B. C. Clark, and R. L. Mercer, *Phys. Rev. C* **47**, 297 (1993).
- [18] L. W. Chen, in *Proceedings of the 14th National Conference on Nuclear Structure in China (NSC2012)* (World Scientific, Singapore, 2012), pp. 43–54.
- [19] M. B. Tsang *et al.*, [arXiv:1204.0466](https://arxiv.org/abs/1204.0466).
- [20] B. Liu, V. Greco, V. Baran, M. Colonna, and M. DiToro, *Phys. Rev. C* **65**, 045201 (2002).
- [21] Z. Y. Ma *et al.*, *Phys. Lett. B* **604**, 170 (2004).
- [22] B. A. Li, *Phys. Rev. C* **69**, 064602 (2004).
- [23] B. A. Li, C. B. Das, S. Das Gupta, and C. Gale, *Phys. Rev. C* **69**, 011603 (2004); *Nucl. Phys. A* **735**, 563 (2004).
- [24] J. Rizzo, M. Colonna, and M. Di Toro, *Phys. Rev. C* **72**, 064609 (2005).
- [25] V. Giordano, M. Colonna, M. DiToro, V. Greco, and J. Rizzo, *Phys. Rev. C* **81**, 044611 (2010).
- [26] L. Ou *et al.*, *Phys. Lett. B* **697**, 246 (2011).
- [27] B. Behera, T. R. Routray, and S. K. Tripathy, *J. Phys. G* **38**, 115104 (2011).
- [28] Z. Q. Feng, *Phys. Rev. C* **84**, 024610 (2011).
- [29] Z. Q. Feng, *Nucl. Phys. A* **878**, 3 (2012).
- [30] B. A. Li and X. Han, *Phys. Lett. B* **727**, 276 (2013).
- [31] X. H. Li *et al.*, *Phys. Lett. B* **721**, 101 (2013).
- [32] X. H. Li *et al.*, [arXiv:1403.5577](https://arxiv.org/abs/1403.5577).
- [33] Y. X. Zhang, M. B. Tsang, Z. X. Li, and H. Liu, *Phys. Lett. B* **732**, 186 (2014).
- [34] W. J. Xie and F. S. Zhang, *Phys. Lett. B* **735**, 250 (2014).
- [35] C. Xu, B. A. Li, and L. W. Chen, *Phys. Rev. C* **82**, 054607 (2010).
- [36] D. D. S. Coupland *et al.*, [arXiv:1406.4546](https://arxiv.org/abs/1406.4546).
- [37] O. Hen *et al.*, [arXiv:1408.0772](https://arxiv.org/abs/1408.0772); *Phys. Rev. C* (to be published).
- [38] J. Xu and C. M. Ko, *Phys. Rev. C* **82**, 044311 (2010).
- [39] R. Chen, B.-J. Cai, L.-W. Chen, B.-A. Li, X.-H. Li, and C. Xu, *Phys. Rev. C* **85**, 024305 (2012).
- [40] J. Xu, L. W. Chen, B. A. Li, and H. R. Ma, *Phys. Rev. C* **75**, 014607 (2007).
- [41] H. Müller and B. D. Serot, *Phys. Rev. C* **52**, 2072 (1995).
- [42] J. Xu, L. W. Chen, B. A. Li, and H. R. Ma, *Phys. Lett. B* **650**, 348 (2007).
- [43] B. A. Li, L. W. Chen, H. R. Ma, J. Xu, and G. C. Yong, *Phys. Rev. C* **76**, 051601(R) (2007).